Matrix Biology 128 (2024) 11–20

Contents lists available at ScienceDirect

Matrix Biology

journal homepage: www.elsevier.com/locate/matbio

A lysyl oxidase-responsive collagen peptide illuminates collagen remodeling in wound healing

Paul Hiebert [a,1], Giuseppe Antoniazzi [b], Matthew Aronoff [b,2], Sabine Werner [a,*], Helma Wennemers [b,*]

[a] Department of Biology, Institute of Molecular Health Sciences, ETH Zurich, Otto-Stern-Weg 7, Zurich 8093, Switzerland
[b] Department of Chemistry and Applied Biosciences, Laboratory of Organic Chemistry, ETH Zurich, Vladimir-Prelog Weg 3, Zurich 8093, Switzerland

ARTICLE INFO

Keywords:
Lysyl oxidase
Collagen
Wound healing
Tissue remodeling
Fibrosis

ABSTRACT

Tissue repair and fibrosis involve the dynamic remodeling of collagen, and accurate detection of these sites is of utmost importance. Here, we use a collagen peptide sensor (**1**) to visualize collagen formation and remodeling during wound healing in mice and humans. We show that the probe binds selectively to sites of collagen formation and remodeling at different stages of healing. Compared to conventional methods, the peptide sensor localizes preferentially to areas of collagen synthesis and remodeling at the wound edge and not in matured fibrillar collagen. We also demonstrate its applicability for *in vivo* wound imaging and for discerning differential remodeling in wounds of transgenic mice with altered collagen dynamics. Our findings show the value of **1** as a diagnostic tool to rapidly identify the sites of matrix remodeling in tissue sections, which will aid in the conception of new therapeutic strategies for fibrotic disorders and defective tissue repair.

List of abbreviations

BAPN	β-aminopropionitrile
caNrf2	constitutively active Nrf2
CMP	collagen model peptide
ECM	extracellular matrix
LOX	lysyl oxidase
Nrf2	nuclear factor erythroid-derived 2-like 2
PBS	phosphate buffered saline
PMT	photomultiplier tube
SHG	second harmonic generation

Introduction

The complex and coordinated process of wound healing is essential for restoring structural integrity and functionality to tissues following injury [1–3]. A key aspect of this process is the dynamic remodeling of the extracellular matrix (ECM), which includes the deposition and maturation of fibrillar collagens that serve as the primary structural component of the ECM in mammals [4]. A proper balance of collagen *de novo* formation and remodeling is essential for successful wound repair. Insufficient or excessive collagen deposition and maturation can lead to pathological conditions, such as chronic, non-healing wounds or hypertrophic scars, respectively [1–3].

Lysyl oxidases (LOX) play a critical role in the collagen maturation process by oxidizing lysine (Lys) or hydroxylysine to allysine residues, thereby initiating cross-linking within and between collagen fibrils as well as within elastin [5]. The precise spatial and temporal regulation of LOX activity during wound healing is, therefore, essential to ensure the proper progression of tissue repair. Abnormal LOX activity has been associated with various pathologies, including fibrotic and malignant diseases, highlighting the importance of understanding and monitoring this process in healthy and diseased tissues [6].

Traditional methods for evaluating collagen remodeling during tissue repair rely on indirect measurements, often based on assessments of tissue histology, collagen concentration, and protease activity [7–9]. These methods lack precision in identifying specific sites and stages of collagen remodeling, and many of them cannot be used in routine diagnostics. Therefore, there is a distinct need for more powerful and nuanced tools.

* Corresponding authors.
E-mail addresses: sabine.werner@biol.ethz.ch (S. Werner), helma.wennemers@org.chem.ethz.ch (H. Wennemers).
[1] Present address: Hull York Medical School, Centre for Biomedicine, Hardy Building, University of Hull, Hull, HU6 7RX, United Kingdom
[2] Present address: Department of Chemistry and Chemical Biology, University of New Mexico, Albuquerque, USA

https://doi.org/10.1016/j.matbio.2024.02.006
Received 30 October 2023; Received in revised form 31 January 2024; Accepted 18 February 2024
Available online 19 February 2024

Previously, we developed a synergistic collagen peptide sensor (probe **1**) that allows for the simultaneous monitoring and targeting of LOX-mediated collagen maturation (Figs. 1A, S1)[10]. This probe binds selectively to and produces a signal at sites of LOX-mediated collagen cross-linking [10]. It has three distinguishing features that, together, set it apart from other existing LOX activity assays: a fluorescence LOX-sensor, a collagen model peptide (CMP), and a chemoselective anchoring moiety (Fig. 1A). The fluorescence sensor lights up upon reaction with LOX, thereby enabling real-time measurement of LOX activity. The collagen model peptide affords the probe with selectivity for collagen, facilitating its preferential non-covalent binding to sites where collagen remodeling takes place [10,11]. Finally, the aminooxy group, the anchor, reacts chemoselectively with aldehydes, the product of LOX, thus, preventing wash-out of the probe (Fig. S1). Combined, the three components equip the probe with the capacity for spatial resolution. We, therefore, envisioned probe **1** as a powerful tool to monitor wound healing. For comparison, we also used a probe that lacks the CMP (probe **2**) (Fig. 1B).

In the current study, we investigated the suitability of the collagen peptide sensor to identify sites of collagen formation and cross-linking in healing skin wounds and for diagnosis of wound healing abnormalities. We show that probe **1** allows, *in situ* and *in vivo*, to detect the location and degree of newly forming and remodeling collagen in wounds at different stages. The probe can even distinguish between normal wound healing and healing with enhanced or reduced scar formation. The utilization of the probe's unique capacity for spatial tracking therefore allows for an improved detection of the timeline of collagen formation and spatial organization of cross-linking as wounds remodel and heal. Therefore, the study puts forth a powerful diagnostic tool for various pathological conditions.

Results

*Differential anchoring kinetics and selective binding of probe **1** in areas of collagen formation and remodeling*

To uncover the dynamics of LOX-mediated collagen cross-linking in wound healing, we initially focused on day 14 of healing of mouse excisional skin wounds (Fig. 2A), a time point at which LOX expression remains elevated (Supplemental Fig. S2A) and the initial formation of scar collagen is underway [7,12,13]. Our investigation drew upon the protocols outlined previously [10]. The procedure involved initial washing of the frozen tissue sections in PBS followed by incubation with **1** (100 μM), for 3 h at 37 °C. To ensure the specificity of the probe for LOX when used on wound sections, we incorporated a pretreatment step with β-aminopropionitrile (BAPN), a potent inhibitor of lysyl oxidases [14,15]. The following blockade of the fluorescent signal validates the specific reactivity of probe **1** with LOX (Fig. 2B). Staining was predominantly observed in the late wound granulation tissue/early scar tissue and around the wound site, suggesting a preference for active zones of collagen remodeling and areas of new collagen formation (Fig. 2B). The protocol was robust, demonstrated through its resistance to alterations in washing times and pre-incubation drying durations, thereby highlighting its reproducibility and ease of use (Supplemental Fig. S2B).

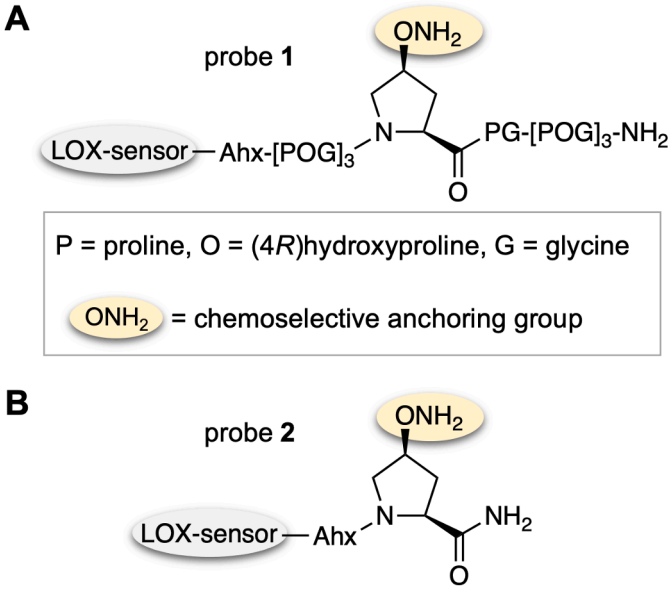

Fig. 1. Collagen peptide-sensor probe **1**. (A) Structure of probe **1**. (B) Structure of probe **2**. Ahx: 6-aminohexanoic acid.

For comparison, we also used probe **2**, which showed lower selectivity for collagen staining in our previous study [10]. We revisited this probe to determine to which extent staining patterns differ in and around wounds, and to differentiate between wound staining due to remodeling collagen versus active LOX. As expected, a much more intensive and broader staining was obtained with **2**, which extended throughout the granulation tissue and was also blocked by pre-treatment with BAPN (Fig. S2C).

Next, we investigated how incubation duration impacts staining. A series of wound serial sections revealed that **1** required more than 60 min for intensive staining (Fig. 2C), while **2** began to exhibit significant staining between 30 and 60 min, with further intensity apparent by the end of the 3 h incubation period (Supplemental Fig. S2D). We then examined whether the limiting factor was the time required for probe anchoring or for subsequent fluorophore unmasking by reaction with LOX. Serial sections were treated with either **1** or **2** for 5 or 30 min to allow for covalent anchoring of the probe, followed by washing and further incubation in PBS until the 3 h mark. After just 5 min of anchoring time followed by subsequent reaction time in PBS, the fluorescent signal of unmasked **1** was already discernable. The signal was significantly amplified when the covalent binding was allowed to proceed for 30 min followed by 2.5 h reaction time in PBS, and it reached its peak when the probe was allowed the full 3 h to anchor and react with LOX (Fig. 2D). This suggests that staining with **1** involves an intricate balance of covalent binding and LOX-reaction time, likely due to its CMP that engages with the remodeling or newly formed collagen, or both. In contrast, the lack of CMP in **2** resulted in rapid anchoring, with intense fluorescence but lower selectivity as early as 5 min (Supplemental Fig. S2E). These findings highlight the nuanced differences in the interaction kinetics of **1** and **2**, reflecting their unique chemistry.

*Selective staining by probe **1** signifies localized collagen remodeling*

Building on these initial findings, we explored staining patterns in wounds in more detail. Staining intensity was quantified across the entire wound section – a range that extended 4 mm to the right and 4 mm to the left of the wound center. Staining intensities to the right and to the left of the wound were averaged to quantify how staining intensity changed as the distance from the center increased.

In wounds 14 days post-injury, the staining intensity profiles for **1** and **2** diverged significantly (Fig. 3A–D). While **1** showed a clear preference for the wound margins and wound interior, **2** displayed staining throughout the wound tissue, and it also stained the adjacent non-wounded skin (Fig. 3A–D). The intensity of **2** staining was also increased in the wound center (Fig. 3A–D), suggesting elevated LOX activity within the wound compared to unwounded skin or abundance of other aldehydes that may react with **2**. Probing sections of normal, unwounded skin revealed an even distribution of both **1** and **2** staining throughout the tissue in the absence of a wound, although **2** staining was again much stronger (Supplementary Fig. S3A–E). The staining intensity of **1** overall was much weaker in normal skin compared to wound tissue

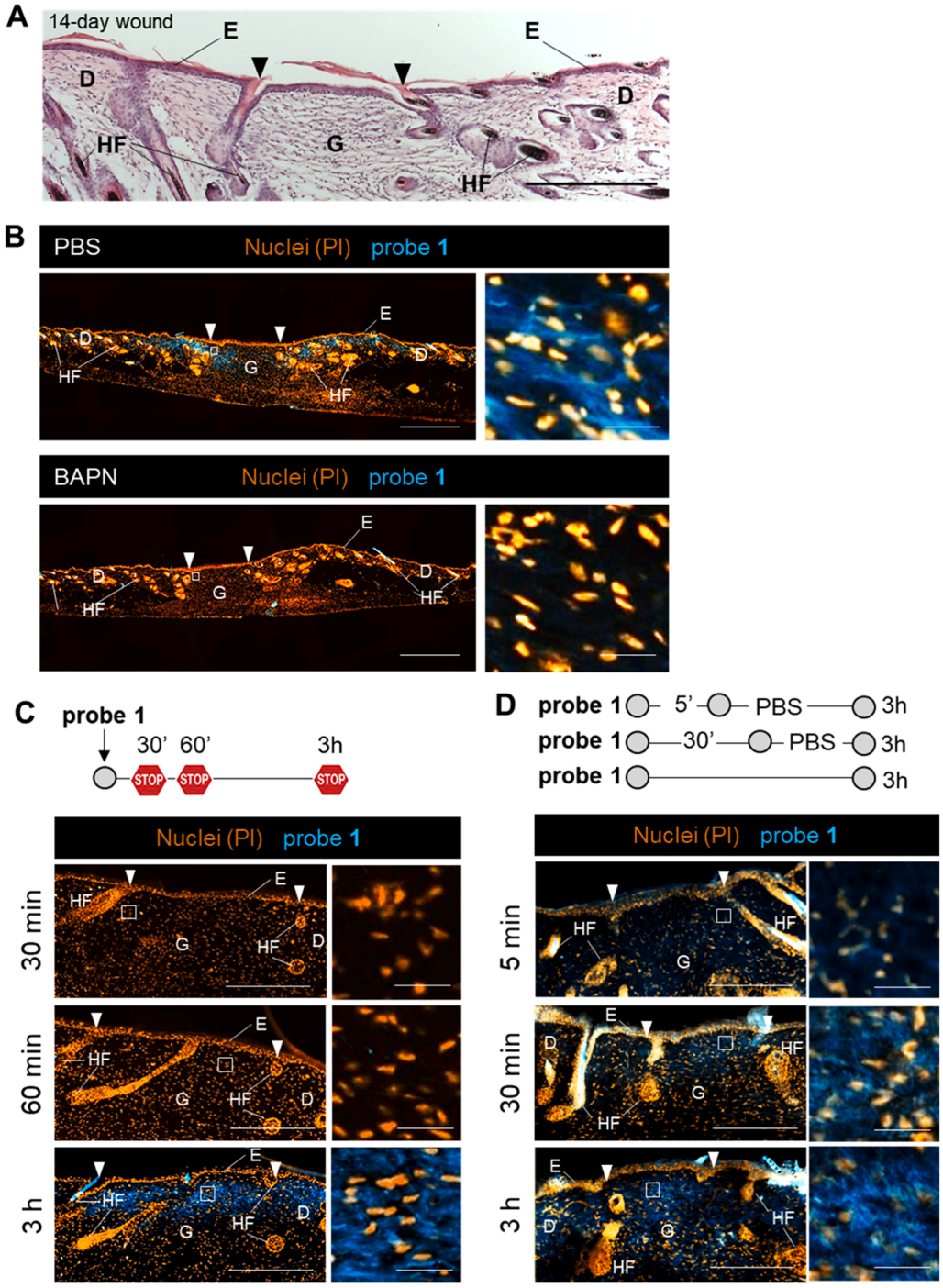

Fig. 2. Disparate anchoring kinetics and favored interaction of probe **1** near wound sites. (A) Representative image of a wound 14 days post wounding stained with hematoxylin and eosin. Black arrowheads indicate the wound margins. D: Dermis; E: Epidermis: G: Granulation tissue; HF: Hair follicle. (B) Representative images of frozen sections from 14-day murine excisional wounds stained with **1** (blue) either with or without pre-treatment with β-aminopropionitrile (BAPN). Nuclei were counterstained with propidium iodide (PI; red). White arrowheads indicate the wound margins. $N = 3$ wounds per group. (C) Representative images of frozen sections from 14-day murine excisional wounds stained with **1** for 30 min, 60 min, or 3 h at 37 °C. $N = 3$ wounds per group. (D) Representative images of frozen sections from 14-day murine excisional wounds, incubated with **1** for different times, followed by subsequent incubation in PBS for a total of 3 h at 37 °C. $N = 3$ wounds per group. Scale bars: 200 μm for whole wound images and 20 μm for zoomed-in images.

(see also comparison of wounded to adjacent normal skin in Fig. 3A), allowing a clear identification of the wound margins.

To better understand the temporal dimension of these probes during wound healing, we expanded our focus to include wounds at 5 days post injury. This time point represents the mid-late stages of the proliferative phase, while the remodeling phase has yet to begin, reflected by the relatively sparse deposition of collagen within the wound [12,16]. At this day, neither **1** nor **2** exhibited staining in the wound center, most likely because of a lack of LOX-generated aldehydes for anchoring (Fig. 3E–G). However, similar to 14-day wounds, a clear divergence in the staining pattern was observed between the compounds, with **1** showing selective staining, primarily around the wound periphery where collagen remodeling is likely underway, while **2** fluorescence was strong throughout the unwounded skin (Fig. 3E).

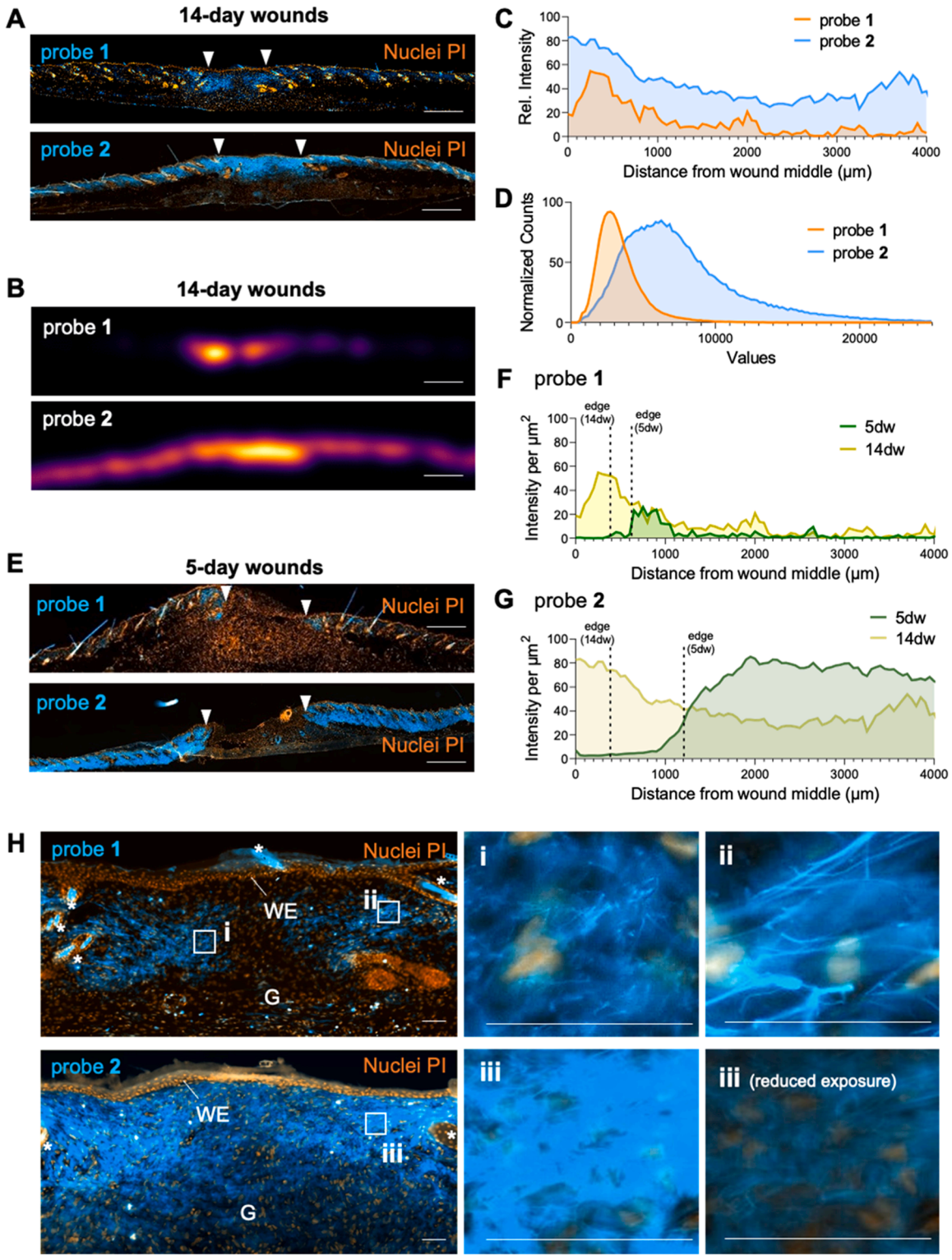

Fig. 3. Localized collagen remodeling indicated by selective probe **1** staining. (A) Representative images of 14-day murine excisional wounds stained with either **1** or **2** (blue). Nuclei were counterstained with propidium iodide (PI; red). White arrowheads indicate the wound margins. $N = 5$ wounds per group. (B) Example density maps based on **1** and **2** staining overlayed on images of 14-day wounds. Representative images of $N = 5$ wounds per group. (C) Normalized quantification of **1** and **2** staining intensity in wound sections. Data is represented as the average of $N = 5$ wounds per group. (D) Histogram of **1** and **2** staining intensities across the entire wound section. Data is represented as the average of $N = 5$ wounds per group. (E) Representative images of 5-day murine excisional wounds stained with either **1** or **2**. $N = 4$ wounds per group. (F) Comparison of **1** staining in 5-day wounds *vs.* 14-day wounds. Data is represented as the average of $N = 4$-5 wounds per group. (G) Comparison of **2** staining in 5-day wounds *vs.* 14-day wounds. Distance from the wound middle is the average value from measurements taken at the right and the left of the wound center. Data is represented as the average of $N = 4$-5 wounds per group. (H) High-resolution images of 14-day wounds stained with **1** or **2**. (i–iii) Zoomed-in images highlighting the staining patterns observed. G: Granulation tissue; WE: Wound epidermis. *Hair/hair follicles. Scale bars: 500 µm (A, B, E), 50 µm (H).

Upon closer examination of the 14-day wound sites, a clear divergence in staining patterns was apparent (Fig. 3H, Supplemental Fig. S3F, G). Areas lit up by **1** showed a fibrous morphology, with the appearance of smaller, fiber-like objects seen more towards the center of the wound (Fig. 3H). In contrast, **2** inside the wound was noticeably diffuse, devoid of the clear, distinct fiber-like patterns exhibited by **1** (Fig. 3H). This diffuse appearance remained, even when exposure was reduced (Fig. 3H). Together, these data reinforce the notion of the discriminatory binding of **1**, indicating areas of newly formed collagen and active collagen remodeling.

*Probe **1** has selectivity for newly formed and remodeling collagen*

Next, we aimed to delineate the specific localities of **1** binding within

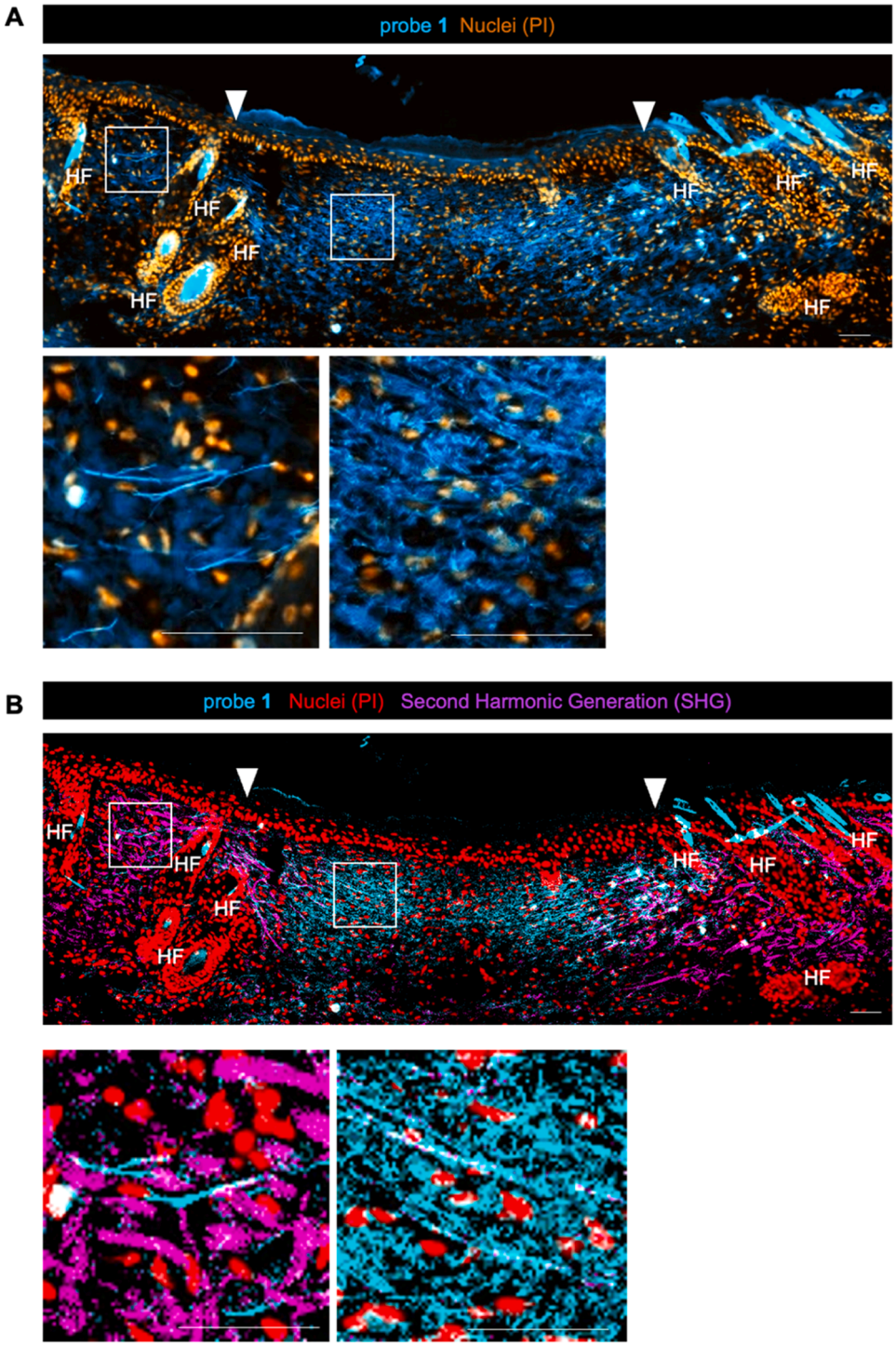

Fig. 4. Probe **1** does not co-localize with mature fibrillar collagen. (A) Representative image of a 14-day murine excisional skin wound stained with **1** (blue) and analyzed using standard fluorescence microscopy. Nuclei were counterstained with propidium iodide (PI; orange). White arrowheads indicate the wound margins. Note the blue autofluorescence of the hair follicles (HF). (B) The same tissue section imaged using confocal microscopy coupled with multi-photon microscopy and second harmonic generation (SHG) to visualize fibrillar collagen. SHG signal appears magenta, while PI-stained nuclei appear orange. Note the blue autofluorescence of the hairs. Scale bars: 100 μm.

and around wound sites. We used second harmonic generation (SHG), which monitors mature, fibrillar collagen [17], and combined it with confocal microscopy imaging. This monitoring allowed the visualization of staining by **1** in relation to mature, fibrillar collagen. The fluorescence emerging from **1**, detected using confocal microscopy, was similar to the signal observed using conventional fluorescence microscopy, albeit with sharper delineation and reduced background interference (Fig. 4A, B).

Intriguingly, in unwounded skin near the edges of the wound, **1** fluorescence was found in close proximity, but not overlaid with mature fibrillar collagen, as visualized by SHG (Fig. 4B). Similarly, strong **1** staining was visualized within the wound despite a complete absence of SHG signal (Fig. 4B). This is indicative of probe **1** binding and anchoring to emerging collagen still in formation and not sufficiently mature to emit SHG signals. When we applied co-staining techniques using antibodies against collagen I or III, probe **1** again demonstrated a targeted staining pattern (Supplementary Fig. S4A, B). This pattern was confined to distinct areas and did not extend to all regions marked by the antibodies within the wound. Furthermore, we saw no discernible bias towards collagen I or III within the wound, suggesting that **1** exhibits a preference for binding to collagen undergoing remodeling, irrespective of the collagen type (Supplementary Fig. S4A, B). There was also no obvious correlation in staining patterns of **1** and elastin (Supplementary Fig. S4C). Unlike **1, 2** exhibited widespread fluorescence staining across both non-wounded skin and wound tissues, overlapping with SHG signals and also extending into areas without such signals (Supplemental Fig. S4D). This revelation further underscores the selectivity and precision of **1** in identifying areas of active collagen formation/remodeling within and around the wound during the healing process. This was further corroborated by analysis of published spatial transcriptomics data of murine skin wounds during an earlier proliferative phase of wound healing [18], which provides a snapshot of sites of heightened expression of the collagen subunit genes *Col1a1, Col1a2, Col3a1*, and of the genes encoding different LOX isoforms within the wound compared to unwounded skin (Supplemental Fig. S5).

*Probe **1** has selectivity for newly formed and remodeling collagen in vivo*

We next sought to investigate whether the probes can monitor LOX-mediated collagen formation and remodeling in live animals. The probes were administered via subcutaneous injection beneath the wound site 14-days post injury, and the wound tissue was harvested 4 h later (Fig. 5A). We noted a clear infiltration of both **1** and **2** into the wound

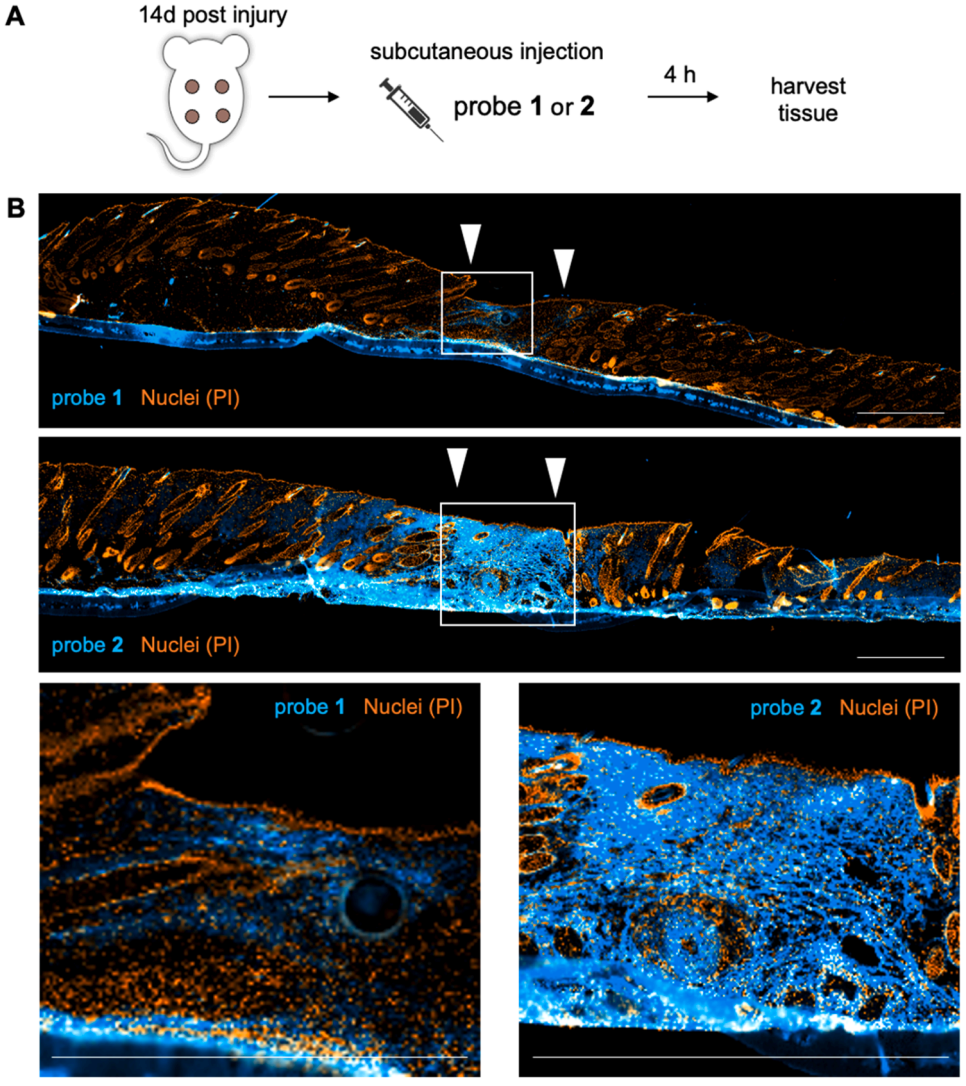

Fig. 5. Probe **1** binds selectively to newly formed and remodeling collagen *in vivo*. (A) Schematic summarizing the experimental procedure. **1** or **2** were injected subcutaneously below the wounds on day 14 after wounding, and tissue was harvested 4 h later. (B) Representative images of 14-day murine excisional wounds injected with either **1** or **2** (blue). Nuclei were stained with propidium iodide (PI; red). White arrowheads indicate the wound margins. Blue autofluorescence along the bottom of the skin/wound results from the underlying paper membrane. Scale bars = 200 μm.

tissue (Fig. 5B). Probe **1** still maintained its enhanced selectivity compared to **2**, which exhibited more generalized staining throughout the wound (Fig. 5B). Intriguingly, **1** lit up newly formed collagen undergoing maturation and remodeling near the wound top (Fig. 5B), despite having earlier access to the ECM in the lower parts of the wound, closer to the site of injection. These observations demonstrate the ability of probe **1** to penetrate tissue and bind only in specific locations. They provide further support for the utility of **1** as a tool to monitor, in real-time, collagen remodeling and progression of collagen formation during wound healing *in vivo*.

*Probe **1** allows detection of differential collagen remodeling in mouse models with altered ECM deposition*

To evaluate whether our probe could discern variations in collagen remodeling during the wound healing process, we made use of available sections from hemizygous transgenic mice expressing a constitutively active mutant of the transcription factor Nrf2 in fibroblasts (caNrf2 mice) in mesenchymal cells, including skin fibroblasts. Expression of the transgene in this cell type was achieved by mating of mice harboring the transgene preceded by a floxed STOP cassette with transgenic mice expressing Cre recombinase under control of the *Col1a2* promoter [12]. In addition, we used hemizygous transgenic mice overexpressing the cytokine activin A in keratinocytes. Both types of mice show wound

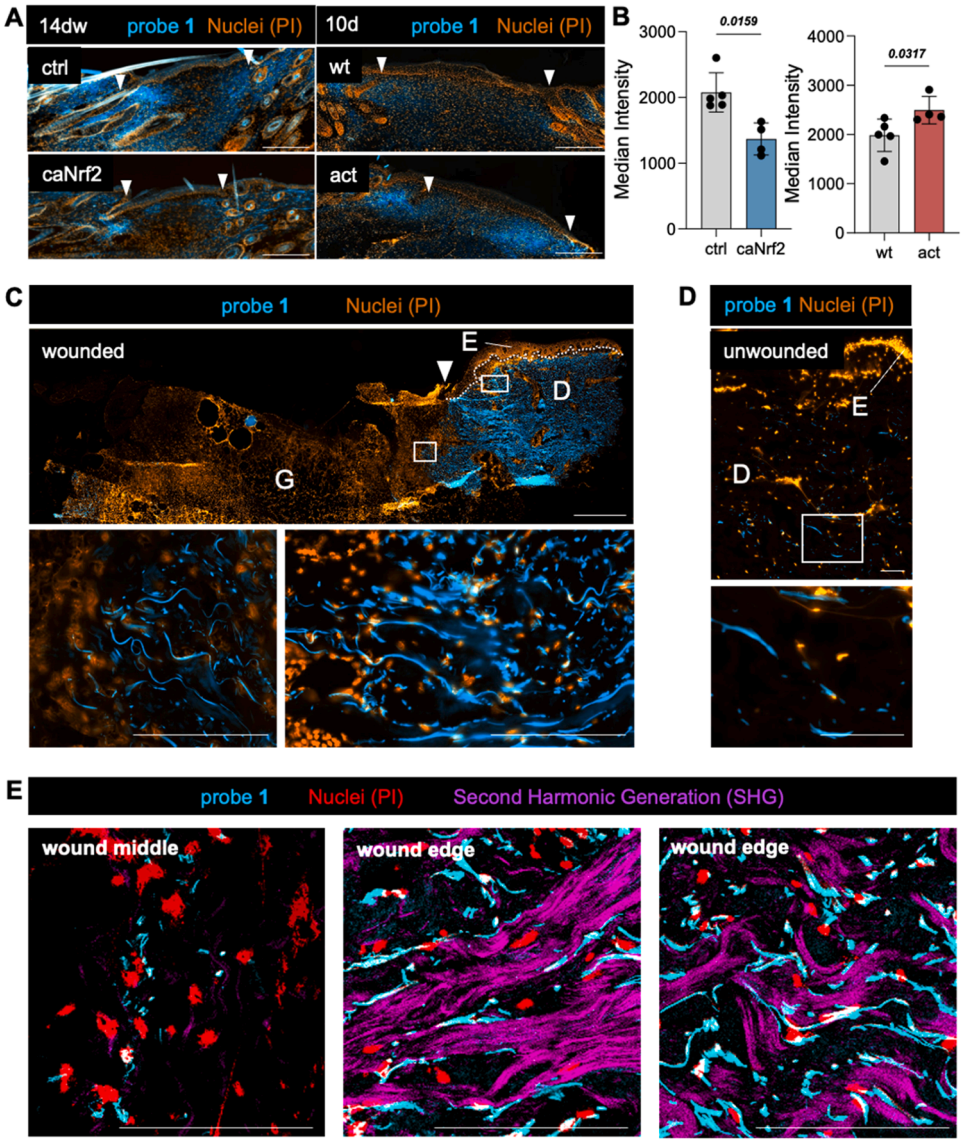

Fig. 6. Differential collagen remodeling in models of altered ECM deposition and in human wounds. (A) Representative images of 14- or 10-day murine excisional wounds from transgenic mice expressing a constitutively active Nrf2 mutant (caNrf2) in fibroblasts or overexpressing activin A in keratinocytes (act) plus their littermate controls (ctrl and wt; Col1a2-Cre mice and wild-type mice, respectively). Wound sections were stained with **1** (blue). Nuclei were stained with propidium iodide (PI; orange). White arrows indicate the wound edges. Scale bars: 200 μm. (B) Quantification of **1** staining intensity within wounds of caNrf2-transgenic and activin A transgenic mice and their control littermates. Bar graphs show mean and SD. $N = 4$-5 per genotype. P-values are indicated above the bars (Mann-Whitney U test). (C) Image of a human excisional wound at day 5 of healing stained with **1** (blue) and counterstained with PI (orange). White arrowhead indicates the wound margin. The area indicated with a rectangle is shown below at higher magnification. Scale bars: 1000 μm or 250 μm (zoomed-in). E: Epidermis; D: Dermis; G: Granulation tissue. (D) Representative image of unwounded, healthy human skin, stained with **1** and counterstained with PI. The area indicated with a rectangle is shown below at higher magnification. E: Epidermis; D: Dermis. Scale bars: 100 μm. (E) Confocal imaging of **1** (blue) in and around a human wound coupled with second harmonic generation multiphoton microscopy to visualize mature fibrillar collagen (magenta). Nuclei were counterstained with PI (red). Wound middle: left panel, wound edge: middle and right panels. Scale bars: 100 μm.

healing alterations, which are, however, only obvious at the histological level. Importantly, they represent distinct ECM phenotypes during wound healing [7,12,19]. Previous experiments have shown that caNrf2 mice exhibit reduced collagen deposition by skin fibroblasts and during wound healing [12], while overexpression of the highly diffusible activin A results in enhanced ECM deposition during the healing process and formation of larger scars [16,19]. Despite the well-characterized wound and ECM phenotypes, details of the remodeling events in these mice remained unknown.

In wounds at 14 days post injury, **1** staining was significantly less intense in caNrf2 mice compared to control mice (Fig. 6A, B). On the other hand, there was a significant increase in **1** staining intensity in activin A overexpressing mice when examining 10-day old wounds in comparison to their controls (Fig. 6A, B). These observations demonstrate the ability of probe **1** to discern variations in collagen formation and remodeling during the wound healing process in different mouse models and even allow quantification of such differences. This result opens up avenues for the use of **1** as a diagnostic tool to probe collagen remodeling dynamics in various physiological and pathological scenarios.

*Probe **1** identifies collagen remodeling patterns in human wounds*

Finally, we set out to investigate how probe **1** performs in the context of human wound healing. In early human wounds, the most robust **1** staining was observed in regions with significant collagen presence near the wound edges (Fig. 6C). Notably, the staining intensity around the wound surpassed that seen in healthy, unwounded human dermis, similar to our observations in mice (Fig. 6C, D).

We once again employed confocal imaging and SHG to visualize **1** staining in the context of fibrillar collagen. Similar to mouse tissue, **1** fluorescence was found in proximity to, but not coinciding with, the SHG signal, consistent with a preference for newly forming/remodeling collagen (Fig. 6E, Supplemental Fig. S6). The **1** signal also appeared to closely align with the SHG-detectable collagen fibers in many cases, suggesting a high degree of interaction with the ongoing collagen fiber formation (Fig. 5E, Supplemental Fig. S6).

In the wound center, where newly forming or remodeling collagen is hardly detectable, **1** staining was scarce (Fig. 6E, left panel), while it was much more intense at the wound edge (Fig. 6E, middle and right panels). This pattern of staining again points to the probe's selectivity for areas of active collagen synthesis and remodeling.

Taken together, these results demonstrate that probe **1** can provide valuable spatial and temporal information about collagen formation and remodeling during the wound healing process in mice and humans.

Discussion

This study has demonstrated the unique ability of collagen peptide sensor **1** to bind to areas of active collagen production and remodeling during murine and human wound healing. When compared with probe **2**, it became evident that all three components of probe **1** – the LOX sensor, the ONH_2 group that covalently anchors the probe into the ECM, and the collagen peptide – are crucial for selective staining. Our results also showcase the ability of **1** to discern between mature, stable collagen, and collagen undergoing cross-linking as part of *de novo* synthesis or remodeling. This unique property was demonstrated in different contexts, including *in situ* studies, *in vivo* animal models, and human wound samples.

While the specificity of probe **1** for newly forming and remodeling tissue areas is clear, it might not detect all aspects of collagen dynamics in wound healing. Although it is established that the remodeling phase of wound healing (e.g. day 14) predominantly involves collagen types I and III [3,20], we cannot rule out that probe **1** binds also to other collagens and possibly also to aldehydes present in other ECM components, although we observed no clear correlation between probe **1** and elastin. Still, at this stage of healing, collagens I and III are particularly abundant ECM proteins within the wound site, and their synthesis and remodeling are actively occurring [3,20]. This contrasts with wounds at day 5, the proliferative phase of healing, where other ECM proteins like fibrin and fibronectin are more prevalent in the wound bed [3,21,22] and where minimal probe **1** staining was observed. Therefore, the clear preference of probe **1** for wounds at day 14, compared to unwounded skin or day 5 wounds, strongly indicates a selectivity for these remodeling collagens.

The relatively high expression and turnover of collagen III in healing wounds, as compared to its presence in healed skin [20], might suggest that probe **1** prefers this collagen type. However, this notion remains speculative at this stage. Co-staining 14-day wounds with probe **1** and antibodies against collagen I and collagen III show the presence of these collagens throughout the wound, corresponding to probe **1** in some areas but not others. Accordingly, probe **1** likely does not discriminate but rather binds areas where both collagen III and I are actively undergoing cross-linking and remodeling. Therefore, the precise molecular binding sites or molecules that are targeted by probe **1** remain to be fully elucidated.

The use of probe **1** on 5- and 14-day mouse wounds sheds light on the sites and nature of collagen remodeling during wound healing. The preferential staining of **1**, in contrast to **2**, in the wound and around the wound edge, points to these regions as hotspots of dynamic collagen synthesis and remodeling. It also shows that the binding and fluorescence of probe **1** depend not only on the amount of collagen but also on the stage of collagen development and turnover. Furthermore, probe **1** staining was often observed near the wound boundaries, appearing to 'migrate' from the wound edge towards the center. This indicates that the initial focus of collagen remodeling is at the wound edges immediately after injury, followed by subsequent propagation inward towards the wound center. This is also consistent with the dynamics of granulation tissue formation [3,23]. The use of probe **1**, therefore, serves to map active sites of collagen remodeling in a temporal and spatial manner.

Current methodologies for assessing collagen remodeling in wounds primarily rely on inferences based on measurements of collagen protein levels, the activity of collagen-degrading proteases, or other indirect markers [7–9]. These techniques generally lack the precision necessary to spatially and temporally delineate areas of active collagen remodeling and maturation. Until now, there has not been a tool comparable to probe **1** that possesses the capability to target and chronicle the activity of collagen remodeling sites. Our data show that probe **1** is highly suitable for this purpose, and we demonstrate its ease of use, robustness to protocol alterations, and high sensitivity. These features make it a valuable tool for researchers aiming to understand the intricacies of collagen remodeling during wound healing and in other physiological and pathological conditions. Furthermore, while probe **2** lacks the selectivity of probe **1** in detecting collagen remodeling sites, it may function as a useful general marker of relative LOX activity *in situ*.

Finally, the sensitivity of probe **1** to detect differential patterns of collagen remodeling in wounds of transgenic mice adds another dimension to its utility as a research tool. These data suggest a certain degree of sensitivity, with probe **1** capable of detecting not merely large differences in wounds at different phases (day 5 vs 14), but also subtle differences in remodeling events that occur during the same wound healing stage. This sensitivity aids in understanding the nuanced variations in the wound healing process and paves the way for using probe **1** as a diagnostic tool in other organs and pathologies as well. This advantage of probe **1**, therefore, extends beyond wound healing models and into the broader realm of diseases characterized by aberrant collagen remodeling, such as fibrotic diseases, solid cancers, and age-related degenerative disorders.

In conclusion, the collagen peptide sensor probe **1**, with its unique ability to map areas of active collagen synthesis and remodeling during wound healing, is a groundbreaking tool that provides direct insight into collagen dynamics across various pathological conditions. Its

robustness, ease of use, and sensitivity make it a significant asset in the quest to comprehend and manipulate the complexities of wound healing and fibrotic diseases.

Experimental procedures

Chemical synthesis

Probes **1** and **2** were prepared as described in Ref. [10].

Animals

Mice were housed and fed according to Swiss federal guidelines. Female wild-type C57BL/6 mice (10 weeks of age) used for wound healing experiments were purchased from Elevage Janvier, Le Genest-Saint-Isle, France. Females were used for these experiments due to reduced fighting, which can damage the skin/wounds. Male *Col1a2*-Cre mice in C57BL/6 background [24] were mated with female transgenic CMVcaNrf2 mice (FVB/N background)[25] to generate mice expressing caNrf2 in mesenchymal cells [12]. Only hemizygous transgenic progeny of the F1 generation were used for experiments, and littermates expressing Cre only were used as controls. Mice overexpressing activin A in keratinocytes (*INHBA* subunit) were generated by breeding hemizygous K14-INHBA mice with wild-type mice (CD1 background) [19]. Progeny hemizygous for the K14-INHBA transgene and wild-type littermates (controls) were used for experiments. All animal experiments were performed in the morning. Mice were housed under specific pathogen-free (SPF) conditions and received water and food *ad libitum*. Mouse maintenance and animal experiments had been approved by the local veterinary authorities (Kantonales Veterinäramt Zürich) after review of a detailed application by an expert panel. All mice were checked for pain symptoms, bleeding, and other health problems at different time points after skin wounding and were sacrificed when symptoms appeared according to the approved protocol.

Wound healing experiments in mice

Mice were anesthetized by intraperitoneal injection of ketamine/xylazine (100 mg ketamine / 5–10 mg xylazine per kg body weight). After shaving, four 5 mm diameter full-thickness wounds were created using a biopsy punch, two wounds on either side of the dorsal midline. Wounds were allowed to heal for either 5 or 14 days, at which point the mice were sacrificed by CO_2 inhalation. Wounds were excised and processed for further analysis. For experiments involving subcutaneous injections, 200 μL of **1** or **2** were injected at concentrations of 100 μM, directly underneath the wound. Mice were sacrificed, and wounds were harvested four hours after injection.

Human wound samples

Human wound samples were obtained anonymously from a healing kinetics study with healthy volunteers (trial number 003WH99) with the aim to study gene/protein expression in human wounds. It was undertaken by SWITCH BIOTECH GmbH, Neuried, Germany, at the Clinic and Polyclinic for Dermatology and Allergology at Biederstein of the Technical University of Munich, Germany, after approval by the local Research Ethics Committee. All individuals had signed informed consent to use their wound material for this purpose. A punch biopsy was taken from the margins of 5-day acute skin wounds, embedded in tissue freezing medium, and sectioned.

Histology and fluorescence

Fresh frozen samples of normal or wounded skin were embedded in tissue freezing medium and sectioned to 7 μm. Following a 30 s wash in phosphate buffered saline (PBS), **1** or **2** were added to the unfixed sections at a concentration of 100 μM and allowed to incubate at 37 °C for 3 h in a humidified chamber. Following incubation with **1** or **2**, slides were washed twice for 30 s in PBS and subsequently fixed for 10 min in ice-cold acetone. After fixation, slides were washed in PBS twice for 30 s, counterstained with propidium iodide, mounted and coverslipped. Identical slides/sections were used for standard fluorescence microscopy and second harmonic generation imaging. Immunofluorescence experiments with antibodies against collagen I and collagen III were performed subsequent to staining with the probe and acetone fixation. The collagen I antibody (SouthernBiotech, Birmingham, AL, Cat# 1310-01) was used at a 1:400 dilution and visualized using an anti-goat secondary antibody conjugated to AF-488 (SouthernBiotech, Cat. # 6460-30) The collagen III antibody (SouthernBiotech, Cat# 1330-01) was used at a 1:200 dilution and visualized using the anti-goat secondary antibody conjugated to AF-488 (see above). Slides imaged using standard fluorescence microscopy were scanned using an Axioscan 7 slide scanner (Carl Zeiss AG, Oberkochen, Germany) at 10x or 40x magnification.

Second harmonic generation imaging

Multiphoton microscopy and SHG imaging were performed on 7 μm thick skin sections using a Leica TCS SP8 microscope (Leica, Wetzlar, Germany) equipped with a 25×0.95 numerical aperture L Water HC PL IRAPO objective and a Mai Tai XF MP laser tunable from 710 to 950 nm (Spectra-Physics, Milpitas, CA). F-SHG images were collected through an aligned condenser (0.55NA), SHG filter (435–455 nm) and photomultiplier tube (PMT). Two-photon autofluorescence (elastin) was visualized through an aligned condenser (0.55NA) and HyD detector unit. Laser power was kept constant throughout each experiment, as were PMT voltage and gain. Leica SP8 LAS X v.3.5.5 software was used to control the instrument and for image acquisition. Image analysis was performed using ImageJ (National Institutes of Health, Bethesda, MD).

Image analysis

Images were analyzed using QuPath [26]. Briefly, areas of interest were annotated around the dermis/wound tissue. Hair follicles were subsequently excluded. The area of interest was then divided into 5 μm tiles and each tile measured for fluorescence intensity. The intensity of each tile was plotted as an individual data point in relation to its distance from the center of the wound. For analysis of intensity specifically in wounds (e.g., caNrf2 and activin A transgenic mice), the total intensity within the wound was measured.

Statistical analysis

Statistical testing was performed using GraphPad Prism software (GraphPad, San Diego, CA). Details of sample size and specific statistical test used are indicated in the figure legends. All p-values below 0.05 are considered significant and are labelled in bold within the figures.

Funding

This work was supported by the Swiss National Science Foundation (Grants TMAG-2_209202/1 to H.W. and 310030-212212/1 to SW), ETH Zurich (Open ETH Project SKINTEGRITY.CH to H.W. and SW) and ETH Postdoctoral Fellowship (M.R.A.).

Declaration of competing interest

The authors have no competing interests.

Data availability

No data was used for the research described in the article.

Acknowledgments

We thank Dr. Alexander Konstantinov, Technical University of Munich, for the human wound samples. H.W. and S.W. are members of the SKINTEGRITY.CH collaborative research program.

Supplementary materials

Supplementary material associated with this article can be found, in the online version, at doi:10.1016/j.matbio.2024.02.006.

References

[1] M. Xue, C.J. Jackson, Extracellular matrix reorganization during wound healing and its impact on abnormal scarring, Adv. Wound Care 4 (3) (2015) 119–136 (New. Rochelle).
[2] G.C. Gurtner, S. Werner, Y. Barrandon, M.T. Longaker, Wound repair and regeneration, Nature 453 (7193) (2008) 314–321.
[3] S.A. Eming, P. Martin, M. Tomic-Canic, Wound repair and regeneration: mechanisms, signaling, and translation, Sci. Transl. Med. 6 (265) (2014) 265sr6.
[4] M.D. Shoulders, R.T. Raines, Collagen structure and stability, Annu. Rev. Biochem. 78 (2009) 929–958.
[5] S.D. Vallet, S. Ricard-Blum, Lysyl oxidases: from enzyme activity to extracellular matrix cross-links, Essays Biochem. 63 (3) (2019) 349–364.
[6] T.R. Cox, D. Bird, A.M. Baker, H.E. Barker, M.W. Ho, G. Lang, J.T. Erler, LOX-mediated collagen crosslinking is responsible for fibrosis-enhanced metastasis, Cancer Res. 73 (6) (2013) 1721–1732.
[7] M.S. Wietecha, M. Pensalfini, M. Cangkrama, B. Muller, J. Jin, J. Brinckmann, E. Mazza, S. Werner, Activin-mediated alterations of the fibroblast transcriptome and matrisome control the biomechanical properties of skin wounds, Nat. Commun. 11 (1) (2020) 2604.
[8] M.S. Agren, R. Schnabel, L.H. Christensen, U. Mirastschijski, Tumor necrosis factor-alpha-accelerated degradation of type I collagen in human skin is associated with elevated matrix metalloproteinase (MMP)-1 and MMP-3 *ex vivo*, Eur. J. Cell Biol. 94 (1) (2015) 12–21.
[9] H. Lintel, D.B. Abbas, D.J. Mackay, M. Griffin, C.V. Lavin, C.E. Berry, N. J. Guardino, J.L. Guo, A. Momeni, D.R. Mackay, M.T. Longaker, D.C. Wan, Topical vanadate improves tensile strength and alters collagen organisation of excisional wounds in a mouse model, Wound Repair Regen. 31 (1) (2023) 77–86.
[10] M.R. Aronoff, P. Hiebert, N.B. Hentzen, S. Werner, H. Wennemers, Imaging and targeting LOX-mediated tissue remodeling with a reactive collagen peptide, Nat. Chem. Biol. 17 (8) (2021) 865–871.
[11] S. Chattopadhyay, K.M. Guthrie, L. Teixeira, C.J. Murphy, R.R. Dubielzig, J. F. McAnulty, R.T. Raines, Anchoring a cytoactive factor in a wound bed promotes healing, J. Tissue Eng. Regen. Med. 10 (12) (2016) 1012–1020.
[12] P. Hiebert, M.S. Wietecha, M. Cangkrama, E. Haertel, E. Mavrogonatou, M. Stumpe, H. Steenbock, S. Grossi, H.D. Beer, P. Angel, J. Brinckmann, D. Kletsas, J. Dengjel, S. Werner, Nrf2-mediated fibroblast reprogramming drives cellular senescence by targeting the matrisome, Dev. Cell 46 (2) (2018) 145. -161 e10.
[13] D.Z. Eichenfield, T.D. Troutman, V.M. Link, M.T. Lam, H. Cho, D. Gosselin, N. J. Spann, H.P. Lesch, J. Tao, J. Muto, R.L. Gallo, R.M. Evans, C.K. Glass, Tissue damage drives co-localization of NF-kappaB, Smad3, and Nrf2 to direct Rev-erb sensitive wound repair in mouse macrophages, eLife 5 (2016).
[14] M. Miana, M. Galan, E. Martinez-Martinez, S. Varona, R. Jurado-Lopez, B. Bausa-Miranda, A. Antequera, M. Luaces, J. Martinez-Gonzalez, C. Rodriguez, V. Cachofeiro, The lysyl oxidase inhibitor beta-aminopropionitrile reduces body weight gain and improves the metabolic profile in diet-induced obesity in rats, Dis. Models Mech. 8 (6) (2015) 543–551.
[15] X. Yang, S. Li, W. Li, J. Chen, X. Xiao, Y. Wang, G. Yan, L. Chen, Inactivation of lysyl oxidase by beta-aminopropionitrile inhibits hypoxia-induced invasion and migration of cervical cancer cells, Oncol. Rep. 29 (2) (2013) 541–548.
[16] M. Pensalfini, E. Haertel, R. Hopf, M. Wietecha, S. Werner, E. Mazza, The mechanical fingerprint of murine excisional wounds, Acta Biomater. 65 (2018) 226–236.
[17] X. Chen, O. Nadiarynkh, S. Plotnikov, P.J. Campagnola, Second harmonic generation microscopy for quantitative analysis of collagen fibrillar structure, Nat. Protoc. 7 (4) (2012) 654–669.
[18] D.S. Foster, M. Januszyk, K.E. Yost, M.S. Chinta, G.S. Gulati, A.T. Nguyen, A. R. Burcham, A. Salhotra, R.C. Ransom, D. Henn, K. Chen, S. Mascharak, K. Tolentino, A.L. Titan, R.E. Jones, O. da Silva, W.T. Leavitt, C.D. Marshall, H. E. des Jardins-Park, M.S. Hu, D.C. Wan, G. Wernig, D. Wagh, J. Coller, J.A. Norton, G.C. Gurtner, A.M. Newman, H.Y. Chang, M.T. Longaker, Integrated spatial multiomics reveals fibroblast fate during tissue repair, Proc. Natl. Acad. Sci. U. S. A. 118 (41) (2021) e2110025118.
[19] B. Munz, H. Smola, F. Engelhardt, K. Bleuel, M. Brauchle, I. Lein, L.W. Evans, D. Huylebroeck, R. Balling, S. Werner, Overexpression of activin A in the skin of transgenic mice reveals new activities of activin in epidermal morphogenesis, dermal fibrosis and wound repair, EMBO J. 18 (19) (1999) 5205–5215.
[20] S.S. Mathew-Steiner, S. Roy, C.K. Sen, Collagen in wound healing, Bioengineering 8 (5) (2021) 63 (Basel).
[21] R.A. Clark, J.M. Lanigan, P. DellaPelle, E. Manseau, H.F. Dvorak, R.B. Colvin, Fibronectin and fibrin provide a provisional matrix for epidermal cell migration during wound reepithelialization, J. Investig. Dermatol. 79 (5) (1982) 264–269.
[22] T.H. Barker, A.J. Engler, The provisional matrix: setting the stage for tissue repair outcomes, Matrix Biol. 60-61 (2017) 1–4.
[23] S. Werner, R. Grose, Regulation of wound healing by growth factors and cytokines, Physiol. Rev. 83 (3) (2003) 835–870.
[24] L. Florin, H. Alter, H.J. Grone, A. Szabowski, G. Schutz, P. Angel, Cre recombinase-mediated gene targeting of mesenchymal cells, Genesis 38 (3) (2004) 139–144.
[25] M. Schafer, H. Farwanah, A.H. Willrodt, A.J. Huebner, K. Sandhoff, D. Roop, D. Hohl, W. Bloch, S. Werner, Nrf2 links epidermal barrier function with antioxidant defense, EMBo Mol. Med. 4 (5) (2012) 364–379.
[26] P. Bankhead, M.B. Loughrey, J.A. Fernandez, Y. Dombrowski, D.G. McArt, P. D. Dunne, S. McQuaid, R.T. Gray, L.J. Murray, H.G. Coleman, J.A. James, M. Salto-Tellez, P.W. Hamilton, QuPath: open source software for digital pathology image analysis, Sci. Rep. 7 (1) (2017) 16878.